



# Dynamic Response and Progressive Collapse of a Long-Span Suspension Bridge Induced by Suspender Loss

Hongfan Wang<sup>1</sup>; Qian Chen, Ph.D.<sup>2</sup>; Anil K. Agrawal, M.ASCE<sup>3</sup>; Sherif El-Tawil, F.ASCE<sup>4</sup>; Baidurya Bhattacharya, F.ASCE<sup>5</sup>; and Waider Wong<sup>6</sup>

**Abstract:** Although long-span suspension bridges play a vital role in the transportation infrastructure, their resistance to disproportionate collapse resulting from locally induced damage has not yet been adequately investigated. In this study, computational simulation is used to shed light on how a prototype long-span suspension bridge responds to sudden loss of suspenders. Several scenarios were considered, with a focus on the total number of suspenders lost, their locations, and mode of removal. An increasing number of suspenders were removed either sequentially (i.e., one at a time) or simultaneously (i.e., multiple suspenders removed at the same time) until progressive collapse of the bridge was triggered. The simulation results showed that the bridge exhibited increasing levels of damage as the number of removed suspenders increased, and that the most critical location for suspender removal was near the middle of the bridge. It is shown that the sequential loss of a group of suspenders led to bridge responses that are almost identical with the simultaneous loss of the same group of suspenders. It is also argued that suspension bridges like the prototype system under consideration are highly robust. DOI: [10.1061/\(ASCE\)ST.1943-541X.0003367](https://doi.org/10.1061/(ASCE)ST.1943-541X.0003367). © 2022 American Society of Civil Engineers.

**Author keywords:** Progressive collapse; Suspension bridge; Suspender loss; Member removal analysis; Nonlinear dynamic analysis.

## Introduction

Long-span bridges, such as cable-stayed bridges, suspension bridges, and arch bridges, play a critical role in the current transportation infrastructure systems. As critical structural components in these long-span bridges, cables, including stay cables, suspenders, and hangers, are designed with high safety factors and are well-protected after installation. However, they are still the most vulnerable structural components during extreme natural events, such as earthquakes and hurricanes, and human-made hazards, e.g., blast, vehicular impact, deliberate cutting, and others. The damage or failure of these slender members may cause severe problems. In July 1940, several suspenders on the first Tacoma Narrows Bridge ruptured because of resonance induced by vortex shedding and

aeroelastic flutter, triggering a progressive collapse of the entire bridge (Starossek 2007). In November 2011, the Kutai Kartanegara Bridge in Indonesia collapsed due to the sudden failure of a suspender clamp in the center span, which led to subsequent suspender unzipping (Kawai et al. 2014). In August 2018, the Morandi Bridge in Italy collapsed after losing a stay cable due to corrosion of the tendons near the top (Calvi et al. 2019). In October 2019, the Nanfang'ao Bridge in Taiwan collapsed after several severely corroded hangers snapped progressively (TTSB 2020). During these catastrophic events, cables failed suddenly. Moreover, the failure was initiated locally in one or multiple cables, which then progressively propagated to the entire bridge.

Existing guidelines that address progressive collapse (e.g., GSA 2003; DOD 2009) were all developed exclusively for buildings, and there are no similar standards or guidelines against progressive collapse of bridges. Cable loss and bridge collapse induced are only mentioned briefly in few guidelines. For example, the Post-Tensioning Institute (PTI) (PTI 2012) stated that the sudden loss of any one cable in a cable-stayed bridge should not lead to the instability of the entire bridge. The European Committee for Standardization (CEN) (CEN 2006) requires that sudden loss of any one tension component should be considered during design as an accidental design situation. In both guidelines, dynamic analysis with a dynamic amplification factor (DAF) is recommended to account for the dynamic effects induced by sudden cable loss. Additionally, PTI (2012) also recommended a nonlinear dynamic analysis to explicitly quantify dynamic effects. It is now common practice in the bridge industry to examine cable loss behavior in long-span bridges during the design stage. However, the results of such studies are rarely made public.

Some investigators have studied the dynamic effects associated with sudden cable loss and the potential progressive collapse of bridges (e.g., Ruiz-Teran and Aparicio 2009; Wolff and Starossek 2009; Mozos and Aparicio 2010a, b; Aoki et al. 2013; Zhou and Chen 2014, 2015; Das et al. 2016; Hoang et al. 2016, 2018;

<sup>1</sup>Postdoctoral Researcher, Dept. of Civil and Environmental Engineering, City College of New York, New York, NY 10031 (corresponding author). ORCID: <https://orcid.org/0000-0001-6854-511X>. Email: hwang2@ccny.cuny.edu

<sup>2</sup>Graduate Student, Dept. of Civil and Environmental Engineering, City College of New York, New York, NY 10031. ORCID: <https://orcid.org/0000-0002-8651-5210>. Email: chenqian022@hotmail.com

<sup>3</sup>Professor, Dept. of Civil and Environmental Engineering, City College of New York, New York, NY 10031. Email: agrawal@ccny.cuny.edu

<sup>4</sup>Antoine E. Naaman Collegiate Professor, Dept. of Civil and Environmental Engineering, Univ. of Michigan, Ann Arbor, MI 48109. Email: eltawil@umich.edu

<sup>5</sup>Professor, Dept. of Civil Engineering, Indian Institute of Technology Kharagpur, Kharagpur, West Bengal 721302, India. ORCID: <https://orcid.org/0000-0002-8758-7486>. Email: baidurya@civil.iitkgp.ac.in

<sup>6</sup>Senior Structural Engineer, Federal Highway Administration, 31 Hopkins Plaza, Suite 1520, Baltimore, MD 21201. Email: waider.wong@dot.gov

Note. This manuscript was submitted on October 18, 2021; approved on February 15, 2022; published online on April 6, 2022. Discussion period open until September 6, 2022; separate discussions must be submitted for individual papers. This paper is part of the *Journal of Structural Engineering*, © ASCE, ISSN 0733-9445.

Kim and Kang 2016; Shoghijavan and Starossek 2018a, b; Zhang et al. 2020). However, these research studies mainly focused on cable-stayed bridges and very few of them on suspension bridges. Lonetti and Pascuzzo (2014) investigated the vulnerability and failure behavior of hybrid cable-stayed suspension bridges subject to failure of cables, including stay cables and hangers. Qiu et al. (2014b) studied the dynamic response of a concrete self-anchored suspension bridge subjected to sudden breakage of a single hanger, and they found that the maximum DAF of the suspender adjacent to the lost hanger was more than the value of 2 recommended by PTI (2012). Based on the same bridge, Qiu et al. (2014a) performed a parametric study on several factors and concluded that the bridge response was significantly affected by flexural stiffness of the main cable, hanger distance, and breakage time of the hanger. Wu et al. (2019) investigated the dynamic behavior of a bridge due to sudden breakage of a corroded hanger. Wu and Qiu (2020) studied the effective load cases and hanger scenarios on the dynamic response of a bridge subjected to abrupt breakage of hangers. Research in the four previously mentioned studies was based on the same concrete self-anchored bridge, and only single- or double-hanger loss cases were considered. Overall, the dynamic response of typical long-span suspension bridges during sudden loss of single or multiple suspenders until progressive collapse and its effect on bridge safety is still unclear, which is of significant concern to the bridge engineering community including asset owners, designers, and practicing engineers.

With the aforementioned concern as motivation, the main objective of this paper is to investigate the dynamic behavior of long-span suspension bridges subjected to a sudden loss of suspenders with a specific focus on the potential for progressive collapse. To achieve this objective, a three-span suspension bridge was selected to serve as a prototype bridge. A three-dimensional (3D) finite-element (FE) explicit model of the prototype bridge was

developed in LS-DYNA R10.0 (LSTC 2020). Confidence in the model was gained by comparing its basic responses against an implicit FE model that was used to design the bridge (provided by the bridge design firm). The behavior of the bridge under dead and live load was analyzed for sudden suspender loss, where the total number and locations of the lost suspenders were simulation parameters. Based on the simulation results, several conclusions about the bridge's behavior during sudden loss of suspenders are presented.

## Prototype Bridge

A three-span suspension bridge shown in Fig. 1 was selected as the prototype bridge. It consists of a 655.32-m-long center span and two 228.60-m-long side spans. The two main cables were designed in a second-degree parabola configuration with a sag to span ratio of 1/10 at the center span, and each main cable was made up of 9,196 No. 6 US gauge galvanized cold-drawn steel wires. The stiffening trusses are Warren type and composed of 142 truss panels. There were 69 pairs of suspenders, and each suspender consisted of four steel ropes. Based on the diameters (denoted by  $\emptyset$ ), these steel ropes can be divided into two types: (1) Type I with  $\emptyset = 58.74$  mm, and (2) Type II with  $\emptyset = 63.50$  mm. In each cable plane, 11 Type II suspenders are located in the middle of the center span, and all remaining suspenders are Type I. The suspender spacing was 15.81 m in the center span and 15.37 m in the two side spans. The two steel towers were 127.43 m high. In the transverse direction, the suspended structure consisted of two stiffening trusses spaced 18.59 m apart, floor trusses spaced 4.57 m apart, and a reinforced concrete deck with a thickness of 20.32 cm. The bridge had four 3.96-m-wide traffic lanes and two 0.94-m-wide sidewalks. There were 11 steel stringers under the deck in the

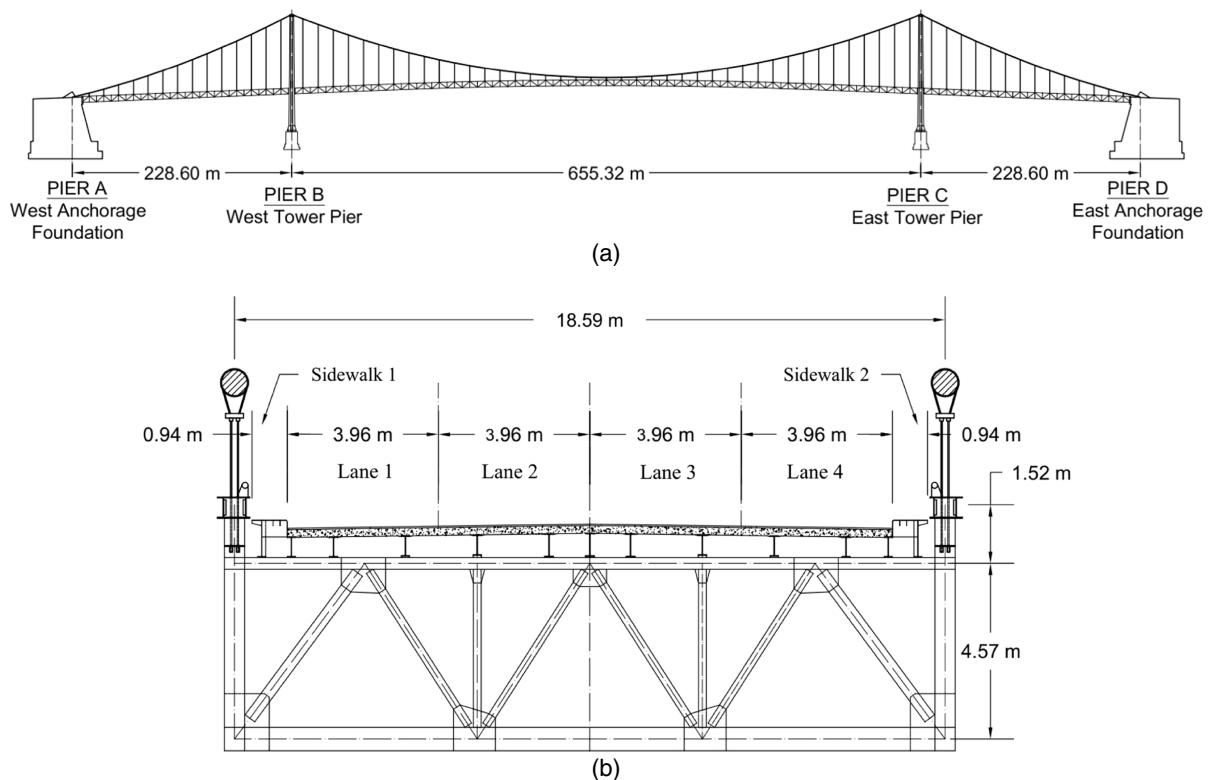
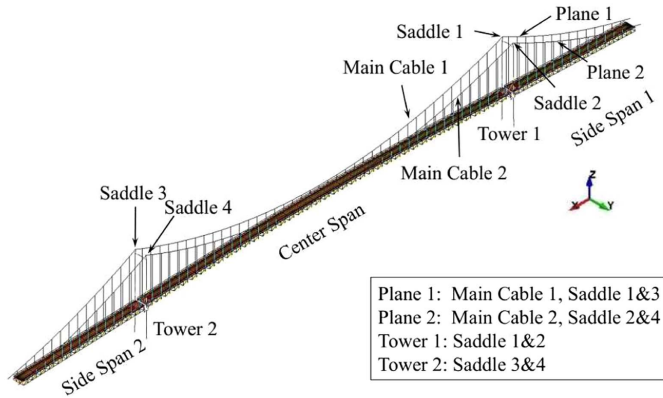


Fig. 1. Prototype bridge: (a) elevation view; and (b) cross section of stiffening trusses.

**Table 1.** Material properties of structural components in the prototype bridge

Structural components	Materials	Young's modulus (GPa)	Compressive strength (MPa)	Yield strength (MPa)	Ultimate strength (MPa)	Failure strain
Towers, stiffening trusses, stringers, and others	ASTM A36	199.95	—	248.21	399.90	0.20
Main cables	Steel wire	193.05	—	1,103.16	1,551.32	0.06
Suspenders	Steel wire	137.90	—	1,103.16	1,551.32	0.062
Deck	Concrete	24.86	27.58	—	—	—

**Fig. 2.** Finite-element model of the prototype bridge.

roadway and two steel stringers under the sidewalks. The material properties of these structural components are listed in Table 1. Further details about the bridge have been given by Agrawal et al. (2021).

## Finite-Element Modeling

The 3D FE model of the prototype bridge is shown in Fig. 2. The element types and material models are summarized in Table 2. Overall, the FE model had 25,898 nodes, 19,928 beam elements, 11,200 shell elements, 6,649 nodal rigid bodies, 2,541 mass elements, and 100 rigid elements.

## Element Naming Scheme

To facilitate reference to the various members of the bridge, the main cable segments and suspenders are designated as shown in

Fig. 3. The main cable (MC) elements are numbered incrementally from left to right, as are the suspender (SUS) cables.

## Component Modeling

### Main Cables and Suspenders

The main cables were modeled by cable elements with properties equivalent to the bundle of wires. A single element was used to model the portion of the main cable between each two adjacent suspenders. The material model `*MAT_PLASTIC_KINEMATIC(003)` was assigned to the cable segments. This material model was selected because of its ability to represent both the plastic kinematic and failure responses of cable materials. As discussed subsequently, pulley elements were introduced between the tower saddles and the adjacent cable elements to simulate the potential slipping of the main cables over the tower saddles. However, because the pulley element was not compatible with elements using `*MAT_003`, the portion of the main cable near the tower saddle was modeled by elastic cable elements with `*MAT_CABLE_DISCRETE_BEAM(071)`, as shown in Fig. 4. Based on the typical stress-strain curve for bridge wires (Mayrbaurl and Camo 2004), the stress-strain curve of the main cables was simplified as bilinear with the material properties in Table 1. Depending on their length, each suspender was modeled by 2–10 resultant truss elements with the material `*MAT_003`. The suspenders' material response was also modeled as bilinear with the properties in Table 1.

### Cable Slippage

When the bridge suffers significant damage, such as the loss of a certain number of suspenders, the main cables may slip over the saddles if the friction force between them is overcome by the unbalanced force across the saddles. Takena et al. (1992) investigated the coefficient of friction between the main cables and tower saddles in several existing long-span suspension bridges with characteristics similar to the prototype bridge. They reported that the friction coefficients were mainly in the range of 0.15 to 0.30. Hence, the median values of 0.21 and 0.20 were taken for the static and

**Table 2.** Element types and material models for the FE model of the prototype bridge

Structural members	Element types	Material model
Main cables (near tower saddles)	Cable	<code>*MAT_CABLE_DISCRETE_BEAM(071)</code>
Main cables (others)	Truss	<code>*MAT_PLASTIC_KINEMATIC(003)</code>
Suspenders	Truss	<code>*MAT_PLASTIC_KINEMATIC(003)</code>
Towers, stiffening trusses, stringers	Belytschko-Schwer resultant beam	<code>*MAT_ELASTIC(001)</code> <code>*MAT_SIMPLIFIED_JOHNSON_COOK(098)</code>
Tower saddles, brackets, and other stiff members	Belytschko-Schwer resultant beam	<code>*MAT_RIGID(020)</code>
Deck	Shell	<code>*MAT_PLASTICITY_COMPRESSION_TENSION(124)</code>
Nonstructural components	Mass	N/A
Connection between main cable and tower saddle	Pulley with friction	N/A
Connection between concrete deck and steel girder	N/A	<code>*CONSTRAINED_NODAL_RIGID_BODY</code>
Connection at internal expansion joints	Discrete beam	<code>*MAT_NONLINEAR_ELASTIC_DISCRETE_BEAM(067)</code>

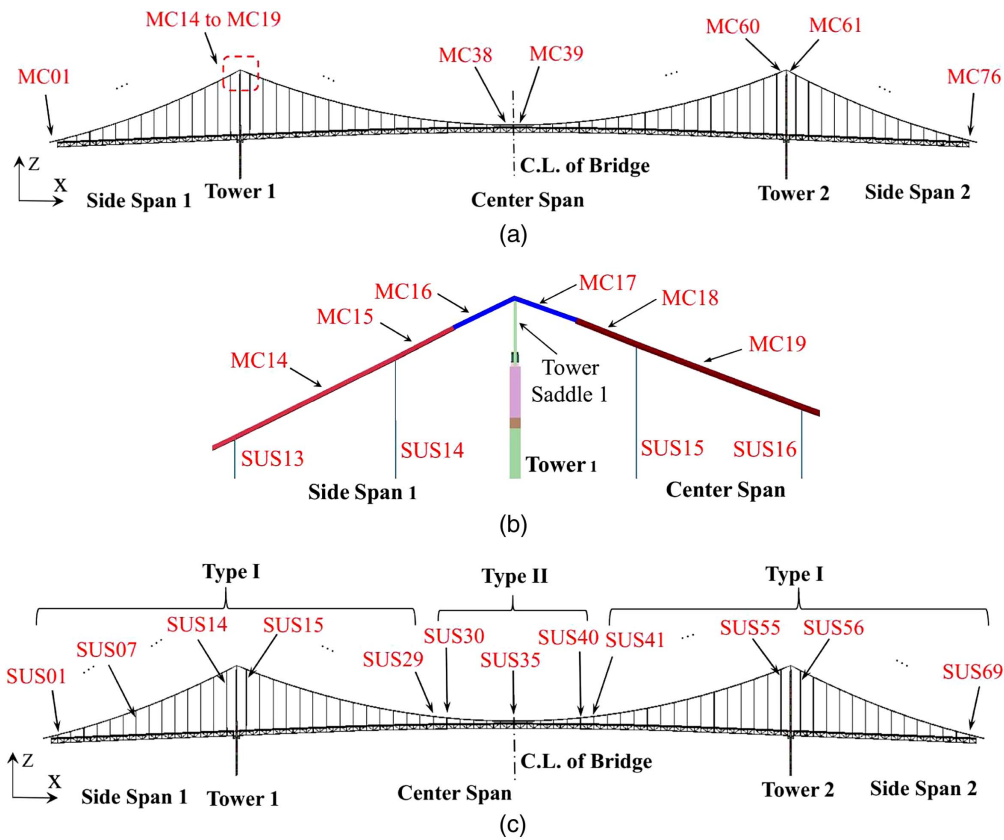


**Fig. 3.** Naming scheme of structural components in the prototype bridge: (a) element IDs of Main Cable 1; (b) main cable elements around Tower 1; and (c) suspenders in Plane 1.

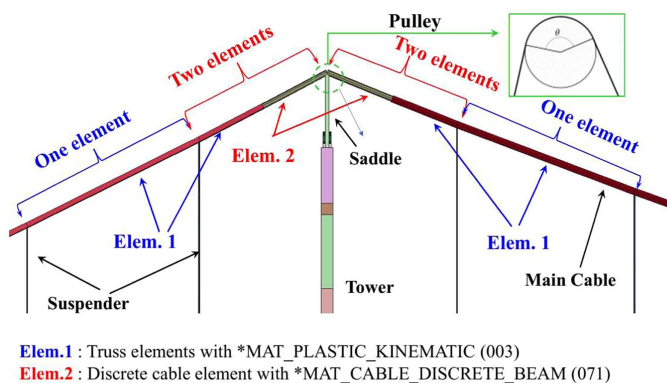


**Fig. 4.** Main cable near tower saddle in the FE model.

dynamic friction coefficients, respectively. To simulate cable slippage, pulley elements (\*ELEMENT\_BEAM\_PULLEY) were added between the tower saddles and the main cable elements near the saddle, as shown in Fig. 4. The pulley elements employed a Coulomb friction model.

### Stiffening Truss

The stiffening truss members were modeled by 3D resultant beam elements with the material model \*MAT\_SIMPLIFIED\_JOHNSON\_COOK (098). The flow stress in \*MAT\_098 can be expressed as  $\sigma_y = (A + B\bar{\epsilon}^n)(1 + C \ln \dot{\epsilon}^*)$ , where  $A$ ,  $B$ ,  $C$ , and  $n$  are input constants,  $\epsilon_0$  is the initial effective plastic strain rate,  $\bar{\epsilon}^p$  is the effective plastic strain,  $\dot{\epsilon}^* = \dot{\epsilon}/EPS0$  is the normalized effective strain

rate, and EPS0 is the quasi-static threshold strain rate (LSTC 2020). Extensive simulation trails resulted in  $A = 249.93$  MPa,  $B = 272.34$  MPa,  $n = 0.328$ ,  $C = 0.0162$ , and  $\epsilon_0 = 0.1/s$ . Also input was the parameter PSFAIL = 0.158. PSFAIL is the effective plastic strain at failure and the value of 0.158 corresponds to an engineering failure strain of 0.20.

Members of the stiffening truss are prone to buckling when subjected to large compressive forces. To model buckling behavior, each member was modeled using two elements and a small initial imperfection (i.e., 1/500 of the member length) was added at mid-member length. This approach follows the method described by Jin and El-Tawil (2003), which was extensively validated using analytical and experimental results.

### Concrete Deck

The concrete deck and the stringers underneath were modeled by shell and beam elements, respectively, and rigid links were added between the nodes of the stringers and the corresponding nodes of the deck to simulate the composite action between them. The material model \*MAT\_PLASTICITY\_COMPRESSION\_TENSION (124) was used to simulate the nonlinear behavior of the concrete deck, such as cracking, crushing, reinforcement yielding, and so on, as done and validated by Alashker et al. (2011). The design details of the deck were not available. Therefore, based on common design details of similar bridge decks, the strengths of concrete and reinforcement were assumed to be 27.58 and 413.69 MPa, respectively. The rebars were assumed to be of No. 6 size with a spacing of 15.24 cm in both longitudinal and transverse directions. The ultimate tensile strain of the deck was assumed to be 0.10. The stress-strain relationship used in \*MAT\_124 for this composite deck is shown in Fig. 5.

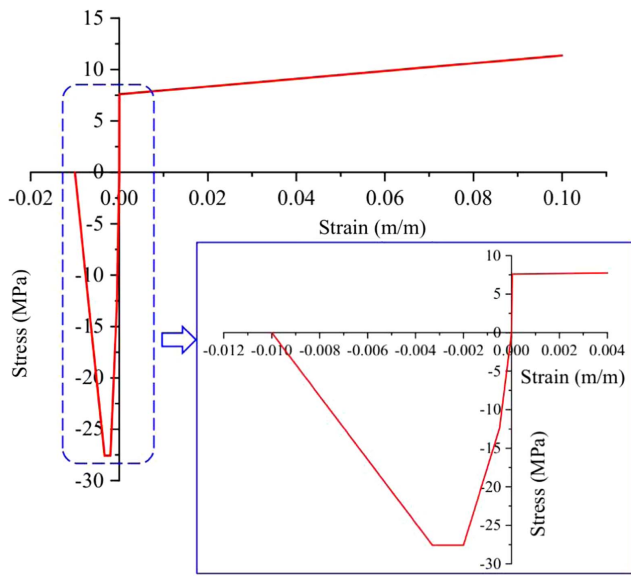


**Fig. 5.** Equivalent stress-strain relationship of \*MAT\_124 for deck elements.

### Interior Expansion Joints

The stringers and deck had a 19.05-mm-wide interior expansion joint (IEJ) after every three truss panels along the longitudinal direction. Stringers were riveted to floor beams at each IEJ. Within these three truss panels, stringers can slide freely in the longitudinal direction on the top of the floor beams. In the FE model, these IEJ were modeled as 19.05-mm gaps in both the concrete deck and stringers, as shown in Fig. 6. Additionally, discrete beam elements were added between the nodes of the two sides of the gap, and the material \*MAT\_NONLINEAR\_ELASTIC\_DISCRETE\_BEAM (067) and force-displacement curves based the axial stiffness of the corresponding concrete deck strip or steel girder were used to simulate the compression-only gap behavior. One such resultant force-displacement curves is shown in Fig. 7, which is based on the axial stiffness of a strip of concrete deck. The small value  $4.45 \times 10^{-4}$

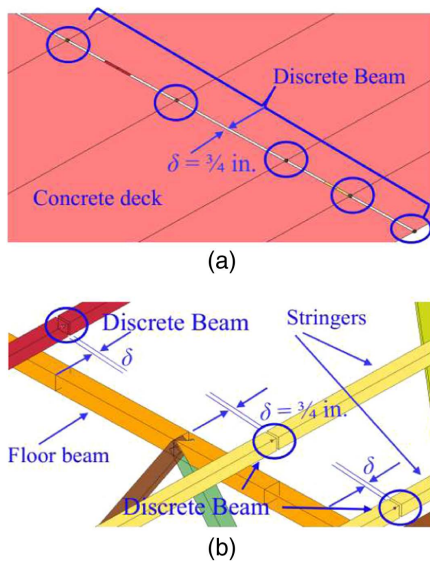


**Fig. 6.** IEJ in the FE model: (a) EIJ between concrete deck panels; and (b) EIJ between stringers.

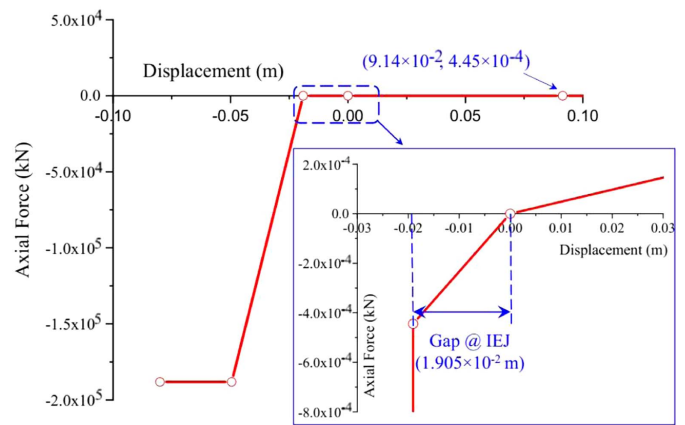


**Fig. 7.** Resultant force-displacement curve of \*MAT\_067 for the non-linear discrete beam at IEJ.

was used to replace zero because the force-displacement curve in \*MAT\_067 does not allow a zero slope.

### Towers

The towers were modeled by 3D resultant beam elements with \*MAT\_098. The tower shafts have a straight tapered box section decreasing from base to top, and the tower struts (i.e., lower and upper cross beams) have a curved tapered box section that decreases from the tower shafts to the bridge center. Thus, they were divided into multiple prismatic elements with different section properties. Each tower shaft was modeled by 26 elements, and each tower strut was modeled by 10 elements.

### Boundary Conditions and Internal Connections

At two ends of the bridge, the splay saddles and concrete anchorage blocks were not modeled. The main cables and stiffening trusses nearby were directly pin connected to the ground, as shown in Fig. 8.

The stiffening trusses were disconnected at the lower strut of each tower. In the vertical direction (+Z-direction), they are supported by the tower links. In the transverse direction ( $\pm Y$ -direction), they were connected to the low tower strut through wind tongues/shoes. With the tooth-type expansion joints, the stringers and deck were disconnected. They were supported on the top of the lower tower shafts vertically and restrained transversely between the two tower shafts. All these internal connections between the suspended structures and the towers were modeled as shown in Fig. 9. The brackets on the tower shafts were modeled as rigid beam elements with negligible mass. Planar joints \*CONSTRAINED\_JOINT\_PLANAR were used to model the connection between the stringer-deck system

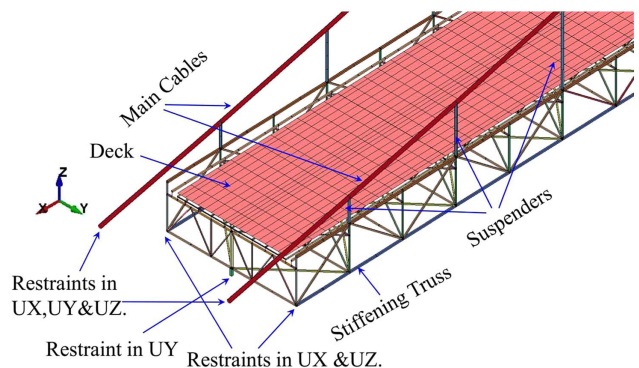


**Fig. 8.** Boundary conditions of the FE model around anchorage.

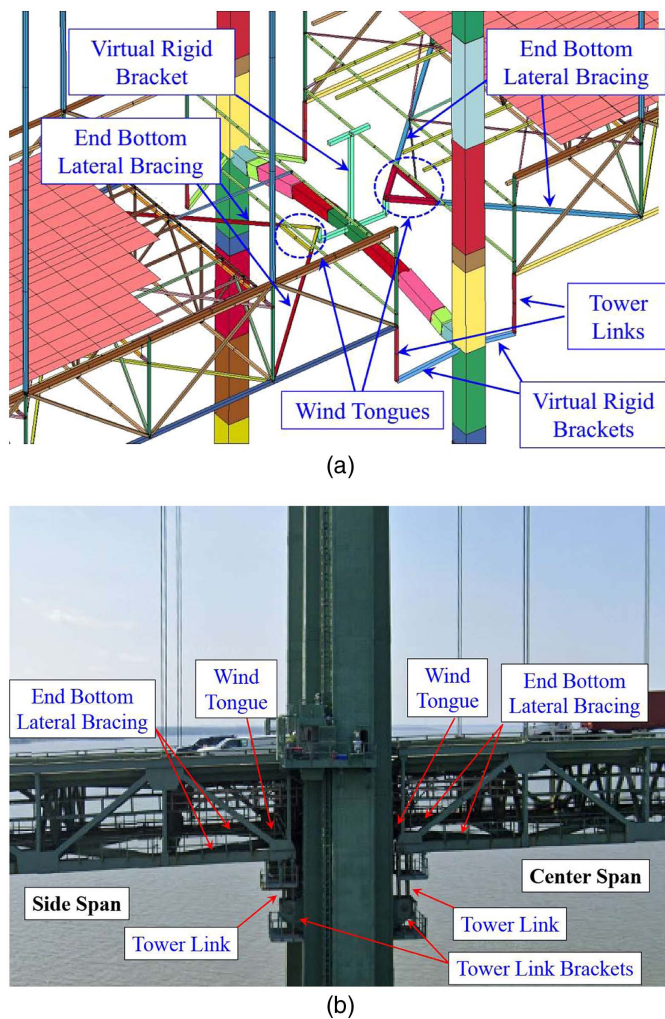


**Fig. 9.** Connection between stiffening trusses and tower at the lower strut: (a) FE model; and (b) prototype bridge (image by Hongfan Wang).

and the tower and the connection between the wind tongues and the lower strut of the towers.

### Developing Confidence in the FE Model

In order to assess the accuracy of the explicit FE model, dead-load analysis was conducted and the results were compared with the results from an implicit FE model that was used to design the bridge (provided by the bridge's design firm). The implicit model was developed in Ansys and was discussed in more detail by Agrawal et al. (2021). The comparison showed close correlation between both models in terms of deflections along the bridge, tension in the main cable, tension in the suspenders, compression in the towers, and mode shapes. Details of this comparison have been given by Agrawal et al. (2021).

The contrast between two models provides some confidence in the explicit model because the theoretical bases and software used for solving both models are different. However, both analyses were based on elastic behavior and did not incorporate material inelasticity or consider the failure response of the bridge. Because there are no available experimental results of a full suspension bridge system that was load tested to failure, it was therefore not possible to validate the overall collapse behavior of the bridge model. Nevertheless, in a simulation, it is common to accept system-level results

as being reasonably representative of reality when the performances of the various components have been separately validated. The authors have successfully validated and utilized many of the models discussed in this paper as done, for example, by Alashker et al. (2011) and Jin et al. (2003) as discussed previously, as well by Khandelwal et al. (2008) for members that yield and undergo fracture. They have also extensively worked with and validated other complex bridge models, e.g., those by Cao et al. (2020, 2021), using the same overall modeling strategy employed herein.

One limitation of the modeling scheme employed in this paper is that joint and connection responses were not modeled. In essence, it was assumed that member failure will occur prior to joint failure and that joint nonlinearity will not contribute substantially to bridge response. This is a common assumption in bridge models of the sort discussed herein. For example, the National Cooperative Highway Research Program (NCHRP) research report 883 (Connor et al. 2018) indicated that a connection failure needs not be modeled if the capacity of the connections were determined to be larger than the individual member, which is typically the case in bridge structures.

### Bridge Response under Dead and Live Loads

The prototype bridge was designed in accordance with the 1961 AASHTO specifications (AASHTO 1961). The design live load (LL) was 32.84 kN/m. Various live-load combinations were considered as discussed by Agrawal et al. (2021), but only the one in which the LL was placed on the entire bridge length along with the dead load (DL) is presented in this paper. This was generally the most critical loading combination. The results for other load combinations have been given by Agrawal et al. (2021). The deflection profiles of the bridge under DL and combined DL and LL are plotted in Fig. 10.

The bridge appears to have an upward deflection under DL. This results from tuning the pretension in the suspenders and main cables in an attempt to match the bridge model's profile with its design profile under DL. When the LL was additionally applied, the entire bridge deflected downward. The maximum negative displacements were  $-42.17$  cm in the center span and  $-21.98$  cm in the side spans, respectively, as measured from the design datum. All displacements discussed next are measured from the design datum shown in Fig. 1.

The tension forces in the main cable are plotted in Fig. 11. Under DL and LL, the tension along the entire main cable increased modestly, by 7.1%–7.4% in each of the side spans and by 14.8%–15.0% in the center span, in comparison with DL alone. The maximum tension was  $1.055 \times 10^5$  kN in MC17 and MC60, which are adjacent to the towers in the center span, and the minimum tension was  $9.398 \times 10^4$  kN in MC01 and MC78,

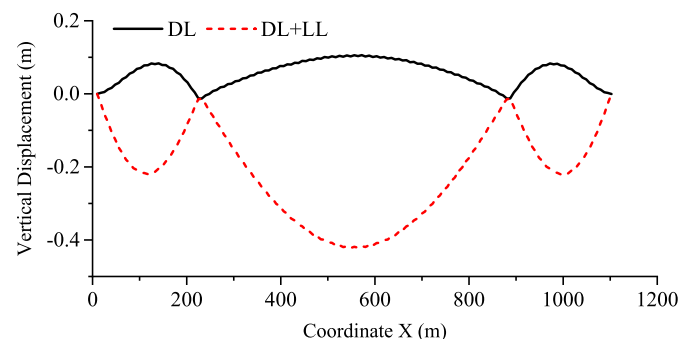


**Fig. 10.** Vertical displacement of the bridge under DL and LL.

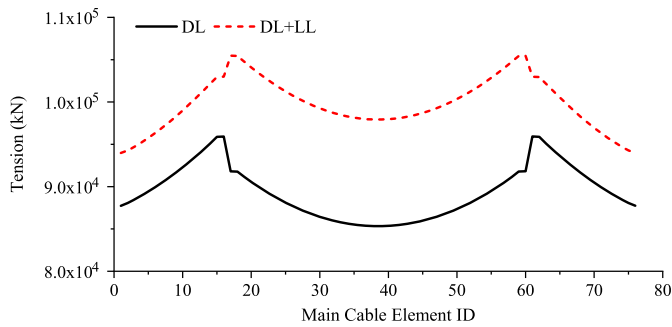


**Fig. 11.** Tensions along a main cable for the bridge under DL and LL.

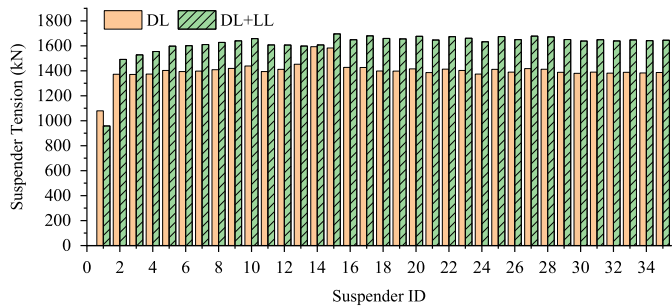


**Fig. 12.** Tension forces in Suspenders SUS01 through SUS35 under DL and LL.

which are near the anchors in the side spans. The tension forces in the suspenders are plotted in Fig. 12. The suspender forces mainly ranged 1,460 to 1,700 kN and saw an increase of 0.9% to 19.0% due to application of LL.

## Bridge Response to the Loss of Multiple Suspenders

The bridge's response to sudden loss of suspenders was investigated through member removal analysis. Depending on the hazard a bridge is subjected to, multiple suspenders may be lost one by one (i.e., sequentially) or multiple suspenders may be lost simultaneously. Both scenarios are feasible and therefore were considered herein. The applied LL was kept constant during the suspender removal process in both scenarios, and the lost suspenders were kept in a single cable plane.

### Case A: Multiple Suspenders Lost Sequentially

This scenario started with a gradual application of both dead and live loads. Once the vibrations due to load application reached steady state, a single suspender was then removed. As the vibrations associated with the shock to the system died down, a second suspender was removed. The process continued until the bridge collapsed.

The damping curve in Fig. 13 was implemented to ensure that the peak dynamic responses were captured in each loading stage and the remaining vibrations were sufficiently damped down in a suitable amount of simulation time. Fig. 13 shows that the load application process was implemented over 18 s with a global damping  $\zeta = 100\%$  of critical. Extensive trials showed that this period of time represented a good balance between computational expediency and reaching a state where vibrational responses were minimal, thus permitting the next step to occur.

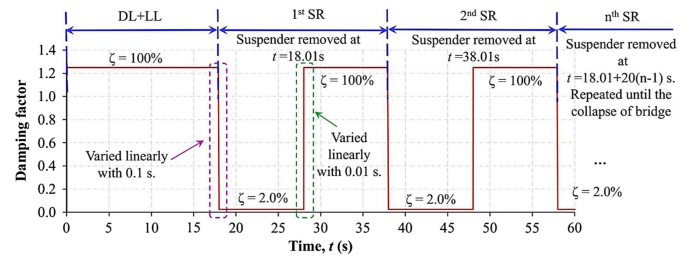


**Fig. 13.** Damping curve in suspender removal analysis.

**Table 3.** Suspender loss scenarios and number of suspenders removed

Scenario No.	Location	First suspender removed	Number of suspenders removed and their range
1	Side Span 1	SUS12	11 (SUS12–SUS02)
2		SUS13	11 (SUS13–SUS03)
3		SUS14	11 (SUS14–SUS04)
4	Center Span	SUS15	11 (SUS15–SUS25)
5		SUS16	11 (SUS16–SUS26)
6		SUS17	11 (SUS17–SUS27)
7		SUS18	11 (SUS18–SUS28)
8		SUS19	10 (SUS19–SUS28)
9		SUS20	9 (SUS20–SUS28)
10		SUS21	9 (SUS21–SUS29)
11		SUS22	9 (SUS22–SUS30)
12		SUS23	9 (SUS23–SUS31)
13		SUS24	9 (SUS24–SUS32)
14		SUS25	9 (SUS25–SUS33)
15		SUS26	9 (SUS26–SUS34)
16		SUS27	9 (SUS27–SUS35)
17		SUS28	9 (SUS28–SUS36)
18		SUS29	8 (SUS29–SUS36)
19		SUS30	8 (SUS30–SUS37)

The first suspender was suddenly removed at 18.01 s, and a simulation duration of 20.0 s (i.e.,  $t = 18.01$ – $38.01$  s) was allowed for the system to reach steady state. The damping was reduced to  $\zeta = 2\%$  of critical at  $t = 18.00$  s and kept constant for the next 10 s of simulation time (i.e.,  $t = 18.01$ – $28.00$  s). The damping was increased once again to  $\zeta = 100\%$  of critical at  $t = 28.01$  s and kept constant for the remaining 9.89 s of the simulation duration (i.e.,  $t = 28.01$ – $37.90$  s) to swiftly reduce the vibrations. Afterward, the damping was reduced again linearly to  $\zeta = 2\%$  at  $t = 38.00$  s for the second suspender removal (SR). Subsequent suspender removals were conducted in the same manner.

### Suspender Loss Scenarios

Due to the symmetry of the bridge and applied loads, the suspenders were removed in Side Span 1 and the part of the center span adjacent to it. Nineteen suspender removal scenarios were modeled as summarized in Table 3, which lists the first suspender removed and the subsequent suspenders that were removed to initiate collapse. The removal process started with the selected suspender closest to Tower 1 then proceeded away from the tower.

Two key observations from the simulation results are as follows: (1) an unzipping-type collapse of the entire bridge was triggered after a critical number of suspenders were removed, and (2) the main cables and towers behaved elastically during the entire process, even at incipient collapse and during the collapse process itself, which saw severe dynamic effects. The number of suspenders removed is designated NSR. Among scenarios listed in Table 3,

**Table 4.** DCR of selected suspenders in Cable Plane 1 near the suspender removal zone

Type	Suspender No.	NSR = 0		NSR = 1 (SUS30)		NSR = 2 (SUS30–SUS31)		NSR = 3 (SUS30–SUS32)		NSR = 4 (SUS30–SUS33)		NSR = 5 (SUS30–SUS34)		NSR = 6 (SUS30–SUS35)		NSR = 7 (SUS30–SUS36)		NSR = 8 (SUS30–SUS37)	
		DCR <sub>p</sub>	DCR <sub>s</sub>	DCR <sub>p</sub>	DCR <sub>s</sub>	DCR <sub>p</sub>	DCR <sub>s</sub>	DCR <sub>p</sub>	DCR <sub>s</sub>	DCR <sub>p</sub>	DCR <sub>s</sub>	DCR <sub>p</sub>	DCR <sub>s</sub>	DCR <sub>p</sub>	DCR <sub>s</sub>	DCR <sub>p</sub>	DCR <sub>s</sub>	DCR <sub>p</sub>	DCR <sub>s</sub>
I	SUS27	0.231	0.230	0.246	0.229	0.245	0.227	0.245	0.227	0.245	0.224	0.274	0.223	0.267	0.218	0.268	0.212	—	—
	SUS28	0.230	0.234	0.250	0.237	0.256	0.239	0.256	0.239	0.268	0.249	0.393	0.348	0.466	0.420	0.541	0.489	—	—
	SUS29	0.227	0.439	0.652	0.449	0.845	0.566	0.845	0.566	1.012	0.677	1.147	0.690	1.248	0.756	1.348	0.834	—	—
	SUS30	0.192	—	—	—	—	—	—	—	—	—	—	—	—	—	—	—	—	—
II	SUS31	0.195	0.380	—	—	—	—	—	—	—	—	—	—	—	—	—	—	—	—
	SUS32	0.193	0.204	0.558	0.392	0.720	0.498	0.720	0.498	0.855	0.607	—	—	—	—	—	—	—	—
	SUS33	0.193	0.201	0.210	0.194	0.210	0.194	0.210	0.194	0.213	0.189	0.215	0.184	0.249	0.213	0.279	0.234	—	—
	SUS34	0.193	0.202	0.205	0.191	0.205	0.192	0.205	0.192	0.213	0.189	0.221	0.183	0.249	0.213	0.279	0.234	—	—
	SUS35	0.193	0.200	0.209	0.192	0.209	0.192	0.205	0.190	0.213	0.189	0.221	0.185	0.249	0.213	0.279	0.234	—	—
	SUS36	0.192	0.198	0.205	0.191	0.205	0.191	0.204	0.189	0.215	0.185	0.219	0.184	0.249	0.213	0.279	0.234	—	—
	SUS37	0.194	0.202	0.206	0.193	0.206	0.193	0.211	0.192	0.213	0.190	0.219	0.185	0.249	0.213	0.279	0.234	—	—
	SUS38	0.193	0.200	0.211	0.193	0.211	0.193	0.215	0.192	0.213	0.190	0.219	0.185	0.249	0.213	0.279	0.234	—	—
	SUS39	0.194	0.201	0.210	0.193	0.210	0.193	0.216	0.192	0.209	0.191	0.220	0.188	0.249	0.213	0.279	0.234	—	—
	SUS40	0.193	0.204	0.210	0.193	0.210	0.193	0.214	0.192	0.217	0.191	0.226	0.189	0.249	0.213	0.279	0.234	—	—

**Progressive collapse**

two scenarios, i.e., Scenario 18 (removal of SUS29–SUS36) and Scenario 19 (removal of SUS30–SUS37), are the most critical because they had the lowest NSR = 8.

**Response of Suspenders**

The demand to capacity ratio (DCR) is used to judge the performance of the suspenders. DCR is defined

$$DCR = \frac{S_d}{F_y} \tag{1}$$

where  $S_d$  = stress in a member after suspender removal; and  $F_y$  = yielding capacity of the structural member. DCR can be used to represent the peak dynamic tensile stress ( $DCR_p$ ) or the steady-state tension ( $DCR_s$ ) reached after suspender removal. The results of these two quantities are summarized in Table 4.

Table 4 indicates that DCR values associated with SUS29 started increasing as Suspenders SUS30 to SUS37 were sequentially removed (i.e., Scenario 19). The values eventually exceeded

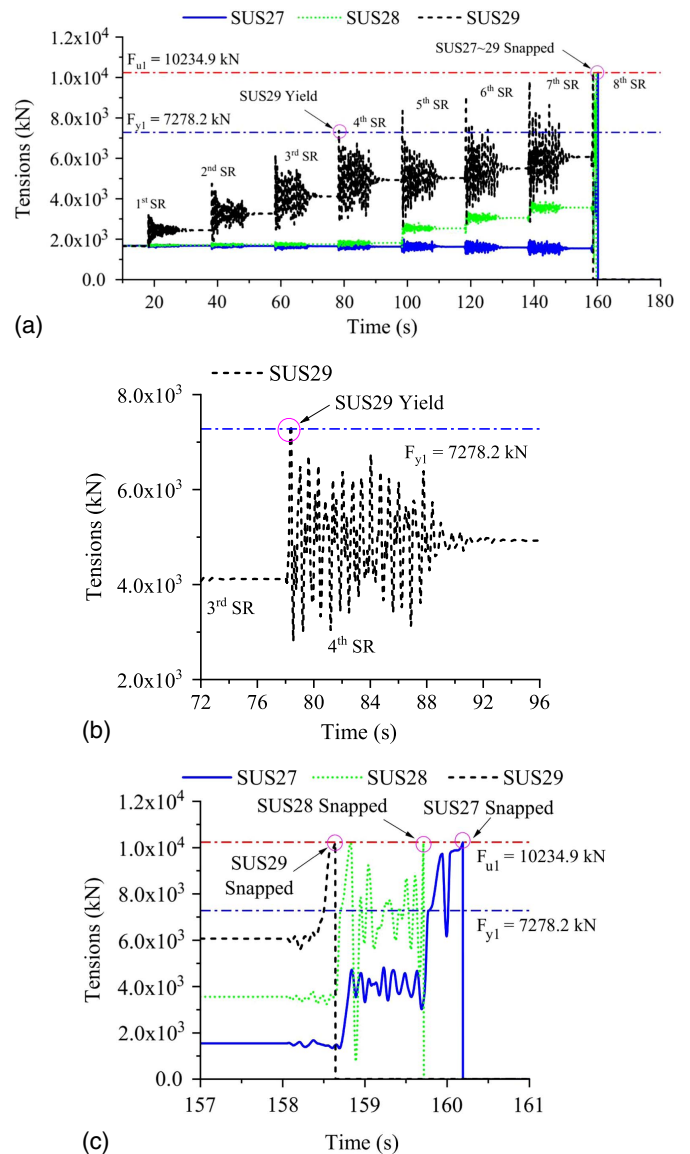


**Fig. 14.** Tension time histories of Suspenders SUS27–SUS29 during multiple suspender removals: (a) Suspenders SUS27–SUS29; (b) yield of Suspender SUS29; and (c) snap of Suspenders SUS27–SUS29.

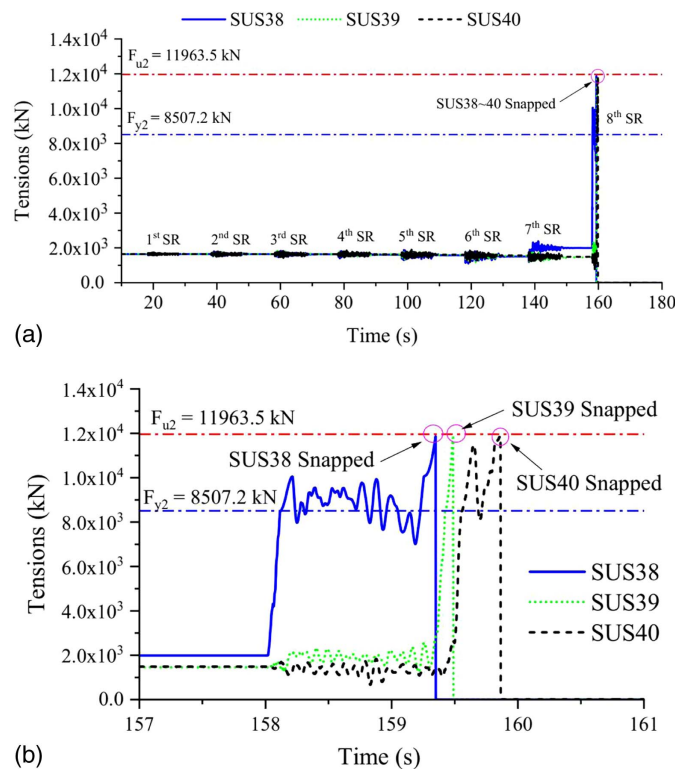
the yield limit of 1.00 for the peak dynamic tension after the removal of SUS33 (i.e., fourth suspender). The stress could exceed the yield limit due to strain rate effects and strain hardening. Adjacent suspenders, i.e., SUS27 and SUS28 were also affected, but the level was dependent on NSR and how close the suspender was to the removal zone.

Fig. 14(a) shows the time histories of the tension forces in Suspenders SUS27–SUS29 as Suspenders SUS30 to SUS37 were sequentially removed. It is clear that the tension increase in SUS29 is much more significant than those in SUS27 and SUS28. Fig. 14(b) shows yielding in SUS29 following the removal of the fourth suspender. Fig. 14(c) shows the snapping of Suspenders SUS27–SUS29. It is observed that SUS29 snapped first, followed by Suspenders SUS28 and SUS27 after the removal of the eighth suspender (when bridge went into suspender unzipping failure).

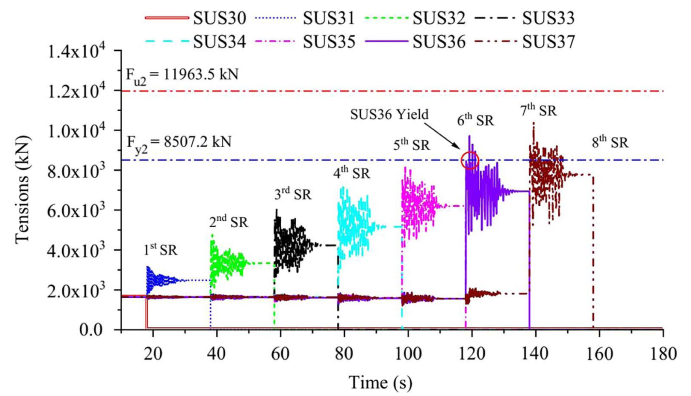
Fig. 15 shows the tension forces and snapping of Suspenders SUS38–SUS40 as Suspenders SUS30–SUS37 were removed. It is again observed that snapping of these suspenders occurred due to a progressive increase in the tension demands after the removal of the eighth suspender.

Fig. 16 shows the increase in tension in Suspenders SUS31–SUS37 as adjacent suspenders were removed. It is observed that the tension in the remaining suspenders in this zone increased progressively as suspenders were removed, and yielding in SUS36 occurred after the removal of the sixth suspender.

Fig. 17 shows the time histories of the tension forces in Suspenders SUS29'–SUS37' (i.e., the suspenders nearby the suspender removal zone in Cable Plane 2) as Suspenders SUS30–SUS37 were removed. Clearly, these suspenders saw much less variation than their counterparts in the main suspender removal plane. Table 5 presents the DCR values of Suspenders SUS 29'–SUS37' during each sudden



**Fig. 15.** Tension time histories of Suspenders SUS38–SUS40 during multiple suspender removals: (a) Suspenders SUS38–SUS40; and (b) snapping of Suspenders SUS38–SUS40.



**Fig. 16.** Tension time histories of Suspenders SUS30–SUS37 during multiple suspender removals.

suspender removal step. Before the progressive collapse was triggered (i.e.,  $NSR \leq 7$ ), the maximum  $DCR_p$  was 0.350 on SUS36', and the maximum  $DCR_s$  was 0.254 on SUS33'.

### Bridge Deflection

The steady-state displacement of the bridge during each SR step before bridge collapse is plotted in Fig. 18. The displacement was measured at the top chord members in each plane of the stiffening truss. Fig. 18 shows that the vertical displacements of the stiffening trusses were localized to the SR zone only and increased with an increase in the number of suspenders removed. The maximum displacement of the intact bridge was  $-0.422$  m in the middle of the center span. After the second SR, the local displacement around SUS30 and SUS31 increased to  $-0.472$  m, developing into the maximum displacement of the entire bridge. Afterward, the maximum displacement of the SR zone dominated the displacement of entire center span until the collapse of the bridge. After the seventh SR, the maximum displacement reached  $-2.590$  m around SUS33 in the damaged steady-state condition. However, the maximum displacement was  $-0.951$  m around SUS33' in Plane 2. Beyond this local zone, the displacement decreased progressively with the removal of more suspenders because the stiffening truss went upward due to the tilting of the suspended structure in the transverse direction.

### Progressive Collapse of the Bridge

As shown in Fig. 14, after the eighth suspender was removed (i.e., SUS37), the tension in SUS29 increased significantly

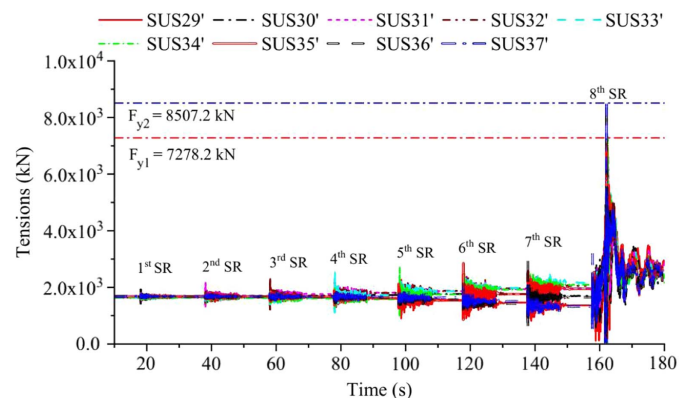


**Fig. 17.** Tension time histories of Suspenders SUS29' – SUS37' during multiple suspender removals.

**Table 5.** DCR of selected suspenders in Cable Plane 2 near the suspender removal zone

Type	Suspender No.	NSR = 0		NSR = 1 (SUS30)		NSR = 2 (SUS30-SUS31)		NSR = 3 (SUS30-SUS32)		NSR = 4 (SUS30-SUS33)		NSR = 5 (SUS30-SUS34)		NSR = 6 (SUS30-SUS35)		NSR = 7 (SUS30-SUS36)		NSR = 8 (SUS30-SUS37)	
		DCR <sub>p</sub>	DCR <sub>s</sub>	DCR <sub>p</sub>	DCR <sub>s</sub>	DCR <sub>p</sub>	DCR <sub>s</sub>	DCR <sub>p</sub>	DCR <sub>s</sub>	DCR <sub>p</sub>	DCR <sub>s</sub>	DCR <sub>p</sub>	DCR <sub>s</sub>	DCR <sub>p</sub>	DCR <sub>s</sub>	DCR <sub>p</sub>	DCR <sub>s</sub>	DCR <sub>p</sub>	DCR <sub>s</sub>
I	SUS29'	0.227	0.228	0.257	0.228	0.254	0.227	0.245	0.224	0.259	0.219	0.310	0.285	0.201	0.272	0.187	0.746		
II	SUS30'	0.192	0.195	0.231	0.195	0.233	0.198	0.227	0.200	0.231	0.203	0.260	0.273	0.208	0.255	0.199	0.605		
	SUS31'	0.195	0.195	0.216	0.195	0.264	0.200	0.249	0.207	0.240	0.213	0.249	0.279	0.228	0.272	0.231	0.733		
	SUS32'	0.193	0.192	0.205	0.192	0.221	0.192	0.278	0.201	0.264	0.212	0.254	0.284	0.231	0.277	0.242	0.775		
	SUS33'	0.193	0.192	0.203	0.192	0.207	0.191	0.229	0.190	0.298	0.203	0.270	0.287	0.232	0.287	0.254	0.786		
	SUS34'	0.193	0.193	0.201	0.193	0.207	0.192	0.213	0.189	0.231	0.186	0.320	0.291	0.226	0.295	0.246	0.858		
	SUS35'	0.194	0.194	0.201	0.194	0.209	0.193	0.215	0.192	0.217	0.186	0.245	0.331	0.203	0.299	0.225	0.845		
	SUS36'	0.192	0.192	0.198	0.192	0.207	0.191	0.206	0.191	0.214	0.188	0.224	0.250	0.163	0.350	0.190	0.995		
	SUS37'	0.194	0.194	0.202	0.194	0.208	0.194	0.212	0.193	0.215	0.192	0.214	0.234	0.173	0.242	0.151	0.995		

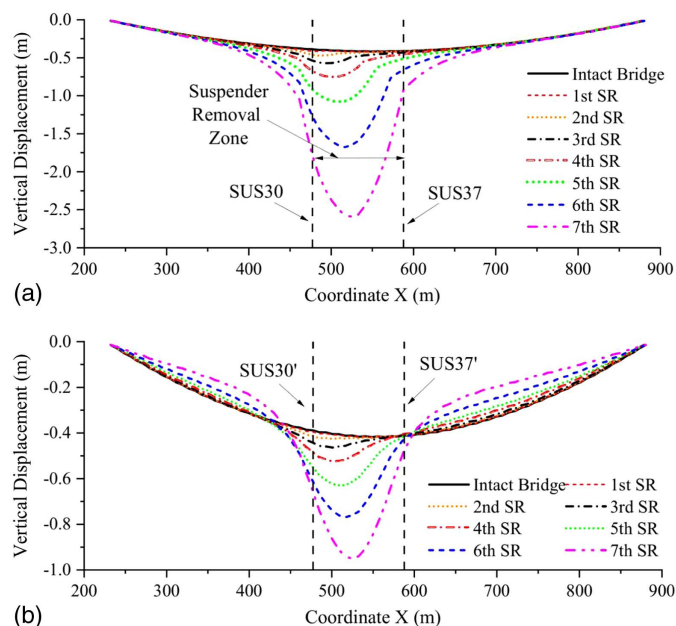


**Fig. 18.** Vertical displacements of stiffening trusses in the center span during multiple suspender removals: (a) Plane 1; and (b) Plane 2.

and reached its ultimate strength of  $F_{u1} = 10,234.9$  kN, leading to a sudden rupture. Subsequently, more suspenders near the suspender removal zone in Plane 1 ruptured one after the other, such as SUS28 and SUS27 as shown in Fig. 14(c) and SUS 38–SUS40 shown in Fig. 15(b), leading to final collapse of the bridge. Fig. 19 shows the final collapse shape of the bridge.

The simulation results show that the main cables started to suffer substantial slip over the tower saddles after the eighth suspender was removed. Prior to that, the cables did not exhibit any slip at all. The time histories of cable slip are shown in Fig. 20. The slipping of main cables continued until the end of the simulation. It was observed from the simulation results that the slipping of the main cables was not unidirectional, i.e., the main cables slipped back and forth over the saddles during the violent collapse process.

### Case B: Bridge Response to Simultaneous Loss of Multiple Suspenders

It is possible that several suspenders of a bridge may be lost simultaneously, instead of sequentially. To investigate this possibility, the seven scenarios in Table 6 were investigated. All suspender losses were in a single cable plane (i.e., Plane 1 only). The suspenders were suddenly removed at 18.01 s after the structure reached steady state after application of the dead and live loads. The damping curve in Fig. 13 was adopted, but the simulation ended at 40.0 s.

The DCR of the suspenders in the vicinity of the suspender removal zone are summarized in Table 7, including the DCR of suspenders in the intact bridge (i.e., NSR = 0) for comparison. By comparing the results for sequential suspender removal in Table 4 with those in Table 7 for simultaneous suspender removal, it is observed that the results for both situations, including the final collapse mechanism, yielded almost identical results. Clearly, the mode of suspender removal did not have a significant effect on the response of the bridge.

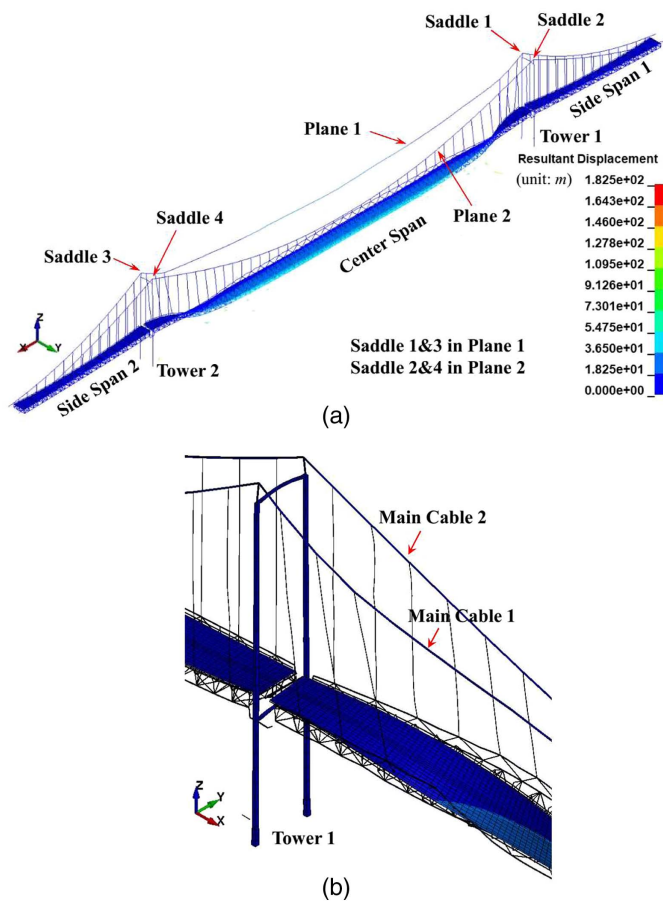


**Fig. 19.** Collapse of entire bridge after the loss of the eighth suspender: (a) global collapse; and (b) close-up view near Tower 1.

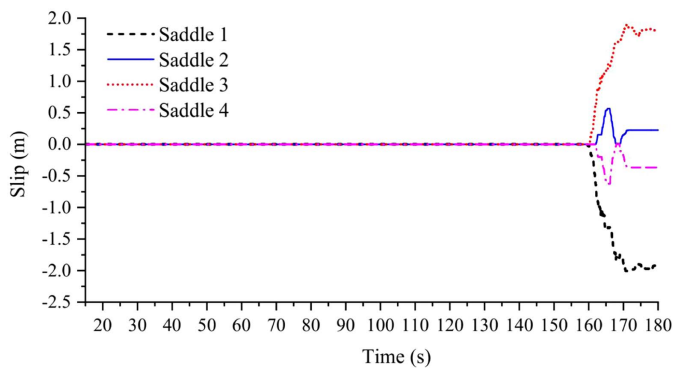


**Fig. 20.** Slip of main cables over tower saddles.

**Table 6.** Scenarios of simultaneous multiple suspenders loss

Scenario No.	NSR	Suspenders lost
B1	2	SUS30 and SUS31
B2	3	SUS30–SUS32
B3	4	SUS30–SUS33
B4	5	SUS30–SUS34
B5	6	SUS30–SUS35
B6	7	SUS30–SUS36
B7	8	SUS30–SUS37

**Table 7.** DCR of selected suspenders near the removal zone in Plane 1 during multiple suspenders lost simultaneously

Type	Suspender No.	NSR = 0		NSR = 2 (SUS30–SUS31)		NSR = 3 (SUS30–SUS32)		NSR = 4 (SUS30–SUS33)		NSR = 5 (SUS30–SUS34)		NSR = 6 (SUS30–SUS35)		NSR = 7 (SUS30–SUS36)		NSR = 8 (SUS30–SUS37)	
		DCR <sub>p</sub>	DCR <sub>s</sub>	DCR <sub>p</sub>	DCR <sub>s</sub>	DCR <sub>p</sub>	DCR <sub>s</sub>	DCR <sub>p</sub>	DCR <sub>s</sub>	DCR <sub>p</sub>	DCR <sub>s</sub>	DCR <sub>p</sub>	DCR <sub>s</sub>	DCR <sub>p</sub>	DCR <sub>s</sub>	DCR <sub>p</sub>	DCR <sub>s</sub>
I	SUS27	0.231	0.240	0.229	0.227	0.239	0.225	0.247	0.223	0.247	0.256	0.217	0.253	0.204	—	—	—
	SUS28	0.230	0.248	0.237	0.239	0.287	0.270	0.394	0.369	0.394	0.466	0.431	0.533	0.475	—	—	—
	SUS29	0.227	0.664	0.449	0.566	1.040	0.651	1.176	0.674	1.176	1.264	0.771	1.355	0.890	—	—	—
II	SUS30	0.192	—	—	—	—	—	—	—	—	—	—	—	—	—	—	—
	SUS31	0.195	—	—	—	—	—	—	—	—	—	—	—	—	—	—	—
	SUS32	0.193	0.580	0.392	0.498	—	—	—	—	—	—	—	—	—	—	—	—
	SUS33	0.193	0.206	0.194	0.762	—	—	—	—	—	—	—	—	—	—	—	—
	SUS34	0.193	0.205	0.191	0.204	0.941	0.611	—	—	—	—	—	—	—	—	—	—
	SUS35	0.193	0.205	0.192	0.190	0.209	0.189	—	—	—	—	—	—	—	—	—	—
	SUS36	0.192	0.204	0.192	0.201	0.204	0.186	1.116	0.708	—	—	—	—	—	—	—	—
	SUS37	0.194	0.200	0.192	0.203	0.200	0.188	0.231	0.210	0.803	—	—	—	—	—	—	—
	SUS38	0.193	0.202	0.193	0.192	0.208	0.189	0.209	0.181	0.228	0.261	0.228	1.326	0.897	—	—	—
	SUS39	0.194	0.206	0.194	0.207	0.212	0.192	0.208	0.184	0.176	0.215	0.213	0.311	0.242	—	—	—

## Redundancy and Robustness of the Prototype Bridge

The simulation results discussed in the preceding sections suggest that the prototype suspension bridge is highly robust against the loss of multiple suspenders. The results of this study indicate that eight suspenders must be lost to cause the bridge to collapse. Other than poor maintenance over many years that could concurrently weaken all of the bridge's suspenders, causing this level of damage to collapse the bridge intentionally or accidentally is difficult due to the large distances involved. Specifically, enough damage must be applied to destroy eight adjacent suspenders in a certain zone of the bridge to cause collapse. This is equivalent to causing damage over the entire height of a 30-story building, an unlikely risk. The same robustness argument can be applied to the main cables and towers. These elements are so strong that they remained elastic as the bridge underwent the strong vibrations associated with collapse. Therefore, although by definition the prototype bridge is nonredundant because loss of the main cables or a tower leg would lead to collapse, it can be argued that the prototype bridge is highly robust.

## Conclusions

In this paper, a detailed 3D explicit finite-element model was developed for a typical long-span suspension bridge. The model was used to investigate the dynamic behavior of the bridge resulting from a sudden loss of suspenders. Several scenarios were considered with a focus on the total number of suspenders lost, their location, and mode of removal. An increasing number of suspenders were removed either sequentially (i.e., one at a time) or simultaneously (i.e., multiple suspenders removed at the same time) until progressive collapse of the bridge was triggered. The simulation results showed that the bridge exhibited increasing levels of damage as the number of removed suspenders increased. The most critical location for suspender removals was near the middle of the bridge, which required the removal of eight suspenders until collapse versus 11 in the side spans or in the central span adjacent to the towers. It was shown that the sequential loss of a group of suspenders led to bridge responses that were almost identical with those arising from the simultaneous loss of the same group of suspenders. It was argued that suspension bridges like the prototype system considered in this paper are highly robust given the difficulty of causing sufficient damage over a large enough region and the high strength of the towers and main cables.

## Data Availability Statement

All data shown in the paper are available from the corresponding author upon reasonable request.

## Acknowledgments

This material is based upon work supported by Federal Highway Administration under Contract No. DTFH61-14-D-00010/693JJ318F000170. Any opinions, findings, and conclusions or recommendations expressed in this publication are those of the authors and do not necessarily reflect the views of the Federal Highway Administration. The US Government does not endorse products, manufacturers, or outside entities. Such names are included here for informational purposes only and are not intended to reflect a preference, approval, or endorsement of any product or entity.

## References

- AASHTO. 1961. *Standard specifications for highway bridges*. Washington, DC: AASHTO.
- Agrawal, A. K., S. El-Tawil, Q. Chen, and H. Wang. 2021. *Redundancy in long span bridges for risk mitigation in a multi-hazard environment*. Washington, DC: Federal Highway Administration.
- Alashker, Y., H. Li, and S. El-Tawil. 2011. "Approximations in progressive collapse modeling." *J. Struct. Eng.* 137 (9): 914–924. [https://doi.org/10.1061/\(ASCE\)ST.1943-541X.0000452](https://doi.org/10.1061/(ASCE)ST.1943-541X.0000452).
- Aoki, Y., H. Valipour, B. Samali, and A. Saleh. 2013. "A study on potential progressive collapse responses of cable-stayed bridges." *Adv. Struct. Eng.* 16 (4): 689–706. <https://doi.org/10.1260/1369-4332.16.4.689>.
- Calvi, G. M., M. Moratti, G. J. O'Reilly, N. Scattarreggia, R. Monteiro, D. Malomo, P. M. Calvi, and R. Pinho. 2019. "Once upon a time in Italy: The tale of the Morandi bridge." *Struct. Eng. Int.* 29 (2): 198–217. <https://doi.org/10.1080/10168664.2018.1558033>.
- Cao, R., A. K. Agrawal, S. El-Tawil, and W. Wong. 2021. "Overheight impact on bridges: A computational case study of the Skagit River bridge collapse." *Eng. Struct.* 237 (Jun): 112215. <https://doi.org/10.1016/j.engstruct.2021.112215>.
- Cao, R., S. El-Tawil, and A. K. Agrawal. 2020. "Miami pedestrian bridge collapse: Computational forensic analysis." *J. Bridge Eng.* 25 (1): 04019134. [https://doi.org/10.1061/\(ASCE\)BE.1943-5592.0001532](https://doi.org/10.1061/(ASCE)BE.1943-5592.0001532).
- CEN (European Committee for Standardization). 2006. *Design of steel structures, Part 1-11: Design of structures with tension components*. Brussels, Belgium: CEN.
- Connor, R. J., F. J. Bonachera Martín, A. Varma, Z. Lai, and C. Korkmaz. 2018. *Fracture-critical system analysis for steel bridges*. NCHRP Rep. No. 883. Washington, DC: Transportation Research Board.
- Das, R., A. D. Pandey, M. J. Mahesh, P. Saini, and S. Anvesh. 2016. "Progressive collapse of a cable stayed bridge." *Procedia Eng.* 144 (2): 132–139. <https://doi.org/10.1016/j.proeng.2016.05.016>.
- DOD (Department of Defense). 2009. *Unified facilities criteria: Design of buildings to resist progressive collapse*. Rep. No. UFC 4-023-03. Washington, DC: DOD.
- GSA (General Services Administration). 2003. *Progressive collapse analysis and design guidelines for new federal office buildings and major modernization projects*. Washington, DC: GSA.
- Hoang, V., O. Kiyomiya, and T. An. 2016. "Experimental and dynamic response analysis of cable-stayed bridge due to sudden cable loss." *J. Struct. Eng.* 62 (1): 50–60. <https://doi.org/10.11532/structcivil.62A.50>.
- Hoang, V., O. Kiyomiya, and T. An. 2018. "Experimental and numerical study of lateral cable rupture in cable-stayed bridges: Case study." *J. Bridge Eng.* 23 (6): 05018004. [https://doi.org/10.1061/\(ASCE\)BE.1943-5592.0001227](https://doi.org/10.1061/(ASCE)BE.1943-5592.0001227).
- Jin, J., and S. El-Tawil. 2003. "Inelastic cyclic model for steel braces." *J. Eng. Mech.* 129 (6): 548–557. [https://doi.org/10.1061/\(ASCE\)0733-9399\(2003\)129:5\(548\)](https://doi.org/10.1061/(ASCE)0733-9399(2003)129:5(548)).
- Kawai, Y., D. Siringoringo, and Y. Fujino. 2014. "Failure analysis of the hanger clamps of the Kutai-Kartanegara Bridge from the fracture mechanics viewpoint." *J. JSCE* 2 (1): 1–6. [https://doi.org/10.2208/journalofjsce.2.1\\_1](https://doi.org/10.2208/journalofjsce.2.1_1).
- Khandelwal, K., S. El-Tawil, and F. Sadek. 2008. "Progressive collapse analysis of seismically designed steel braced frames." *J. Constr. Steel Res.* 65 (3): 699–708. <https://doi.org/10.1016/j.jcsr.2008.02.007>.
- Kim, S., and Y. J. Kang. 2016. "Structural behavior of cable-stayed bridges after cable failure." *Struct. Eng. Mech.* 59 (6): 1095–1120. <https://doi.org/10.12989/sem.2016.59.6.1095>.
- Lonetti, P., and A. Pascuzzo. 2014. "Vulnerability and failure analysis of hybrid cable-stayed suspension bridges subjected to damage mechanisms." *Eng. Fail. Anal.* 45 (Sep): 470–495. <https://doi.org/10.1016/j.engfailanal.2014.07.002>.
- LSTC (Livermore Software Technology Corporation). 2020. "LS-DYNA® keywords user manual Volume II-Material models." Accessed September 9, 2020. [https://www.dynasupport.com/manuals/ls-dyna-manuals/ls-dyna\\_manual\\_volume\\_i\\_r12.pdf](https://www.dynasupport.com/manuals/ls-dyna-manuals/ls-dyna_manual_volume_i_r12.pdf).

- Maybaurl, R. M., and S. Camo. 2004. *Guidelines for inspection and strength evaluation of suspension bridge parallel-wire cables*. NCHRP Rep. No. 534. Washington, DC: Transportation Research Board.
- Mozos, C. M., and A. C. Aparicio. 2010a. "Parametric study on the dynamic response of cable stayed bridges to the sudden failure of a stay, Part I: Bending moment acting on the deck." *Eng. Struct.* 32 (10): 3288–3300. <https://doi.org/10.1016/j.engstruct.2010.07.003>.
- Mozos, C. M., and A. C. Aparicio. 2010b. "Parametric study on the dynamic response of cable stayed bridges to the sudden failure of a stay, Part II: Bending moment acting on the pylons and stress on the stays." *Eng. Struct.* 32 (10): 3301–3312. <https://doi.org/10.1016/j.engstruct.2010.07.002>.
- PTI (Post-Tensioning Institute). 2012. *Recommendations for stay-cable design, testing and installation*. Phoenix, AZ: Cable-Stayed Bridges Committee.
- Qiu, W., M. Jiang, and C. Huang. 2014a. "Parametric study on responses of a self-anchored suspension bridge to sudden breakage of a hanger." *Sci. World J.* 2014 (Jan): 11. <https://doi.org/10.1155/2014/512120>.
- Qiu, W., M. Jiang, and Z. Zhang. 2014b. "Responses of self-anchored suspension bridge to sudden breakage of hangers." *Struct. Eng. Mech.* 50 (2): 241–255. <https://doi.org/10.12989/sem.2014.50.2.241>.
- Ruiz-Teran, A. M., and A. C. Aparicio. 2009. "Response of under-deck cable-stayed bridges to the accidental breakage of stay cables." *Eng. Struct.* 31 (7): 1425–1434. <https://doi.org/10.1016/j.engstruct.2009.02.027>.
- Shoghijavan, M., and U. Starossek. 2018a. "An analytical study on the bending moment acting on the girder of a long-span cable-supported bridge suffering from cable failure." *Eng. Struct.* 167 (Mar): 166–174. <https://doi.org/10.1016/j.engstruct.2018.04.017>.
- Shoghijavan, M., and U. Starossek. 2018b. "Structural robustness of long-span cable-supported bridges in a cable-loss scenario." *J. Bridge Eng.* 23 (2): 04017133. [https://doi.org/10.1061/\(ASCE\)BE.1943-5592.0001186](https://doi.org/10.1061/(ASCE)BE.1943-5592.0001186).
- Starossek, U. 2007. "Typology of progressive collapse." *Eng. Struct.* 29 (9): 2302–2307. <https://doi.org/10.1016/j.engstruct.2006.11.025>.
- Takena, K., M. Sasaki, K. Hata, and K. Hasegawa. 1992. "Slip behavior of cable against saddle in suspension bridges." *J. Struct. Eng.* 118 (2): 377–391. [https://doi.org/10.1061/\(ASCE\)0733-9445\(1992\)118:2\(377\)](https://doi.org/10.1061/(ASCE)0733-9445(1992)118:2(377)).
- TTSB (Taiwan Transportation Safety Board). 2020. *Final report on nan-fangao sea-crossing bridge collapse*. Rep. No. TTSB-HOR-20-11-001. Taipei, Taiwan: TTSB.
- Wolff, M., and U. Starossek. 2009. "Cable loss and progressive collapse in cable-stayed bridges." *Bridge Struct.* 5 (1): 17–28. <https://doi.org/10.1080/15732480902775615>.
- Wu, G., and W. Qiu. 2020. "Effect of load cases and hanger-loss scenarios on dynamic responses of the self-anchored suspension bridge to abrupt rupture of hangers." *J. Perform. Constr. Facil.* 34 (5): 04020081. [https://doi.org/10.1061/\(ASCE\)CF.1943-5509.0001482](https://doi.org/10.1061/(ASCE)CF.1943-5509.0001482).
- Wu, G., W. Qiu, and T. Wu. 2019. "Nonlinear dynamic analysis of the self-anchored suspension bridge subjected to sudden breakage of a hanger." *Eng. Fail. Anal.* 97 (Mar): 701–717. <https://doi.org/10.1016/j.engfailanal.2019.01.028>.
- Zhang, Y., Z. Fang, R. Jiang, Y. Xiang, H. Long, and J. Lu. 2020. "Static performance of a long-span concrete cable-stayed bridge subjected to multiple-cable loss during construction." *J. Bridge Eng.* 25 (3): 04020002. [https://doi.org/10.1061/\(ASCE\)BE.1943-5592.0001529](https://doi.org/10.1061/(ASCE)BE.1943-5592.0001529).
- Zhou, Y., and S. Chen. 2014. "Time-progressive dynamic assessment of abrupt cable-breakage events on cable-stayed bridges." *J. Bridge Eng.* 19 (2): 159–171. [https://doi.org/10.1061/\(ASCE\)BE.1943-5592.0000517](https://doi.org/10.1061/(ASCE)BE.1943-5592.0000517).
- Zhou, Y., and S. Chen. 2015. "Numerical investigation of cable breakage events on long-span cable-stayed bridges under stochastic traffic and wind." *Eng. Struct.* 105 (Dec): 299–315. <https://doi.org/10.1016/j.engstruct.2015.07.009>.